IOP Publishing Smart Materials and Structures
Smart Mater. Struct. **30** (2021) 035027 (11pp) https://doi.org/10.1088/1361-665X/abe182

Smart polyimide with recovery stress at the level of high temperature shape memory alloys

Deyan Kong[1], Jie Li[2], Anru Guo[2], Jianxin Yu[3] and Xinli Xiao[1]

[1] MIIT Key Laboratory of Critical Materials Technology for New Energy Conversion and Storage, School of Chemistry and Chemical Engineering, Harbin Institute of Technology, No. 92 West Dazhi Street, Harbin 150001, People's Republic of China
[2] Aerospace Research Institute of Materials & Processing Technology, No. 1 South Dahongmen Road, Fengtai District, Beijing 100076, People's Republic of China
[3] Center of Analysis and Measurement, Harbin Institute of Technology, No. 92 West Dazhi Street, Harbin 150001, People's Republic of China

E-mail: xiaoxinli@hit.edu.cn

Received 30 October 2020, revised 22 January 2021
Accepted for publication 29 January 2021
Published 12 February 2021

Abstract

Recovery stress is important for smart shape memory materials (SMMs) and low recovery stress of shape memory polymers hinders their applications badly, while high temperature shape memory alloys (HTSMAs) are very difficult to be obtained. In order to obtain high temperature SMM with high recovery stress, convenient preparation methods, low cost and good workability, shape memory polyimide with high recovery stress (HRSMPI) at the level of HTSMA is prepared by reinforcing smart polyimide matrix with carbon fiber cloth (CFC) in common lab furnace. The HRSMPI possesses unique sandwich structure with good interfacial bonding between the matrix and filler. It exhibits high glass transition temperature of 300 °C, shape fixity of 90.6% and shape recovery of 92.2%. The recovery stress of HRSMPI is 116 MPa, close to those of some HTSMAs. The primitive actuator made of HRSMPI can overturn metal sheet 147 times heavier than itself, similar to the commercial TiNiHf HTSMA. Meanwhile, its density is 0.96 g cm^{-3}, less than 1/6 of that of TiNiHf. The elastic strain energy is mainly stored in CFC and then released as recovery stress under constrained shape recovery, and HRSMPI has great potential in practical applications.

Supplementary material for this article is available online

Keywords: shape memory polymer, recovery stress, high temperature, shape memory alloy, polyimide, carbon fiber cloth

(Some figures may appear in colour only in the online journal)

1. Introduction

Shape memory materials (SMMs) are smart materials that possess shape memory effect [1–3]. This characteristic is defined in terms of shape fixity and shape recovery [4–6]. Shape fixity means that they can be transformed into other shapes and then fix the temporary shapes, while shape recovery means that they can return to the original shape under suitable stimuli such as heat, electric and magnetic fields [7–10]. Recovery stress is the stress generated when shape recovery is performed under constraint, and it is crucial for SMM since high recovery stress can produce large force to output work in practical applications [11]. The TiNi shape memory alloy (SMA) with recovery stress of 200–760 MPa is the most widely used SMM, and it has found applications in fields like aerospace, medical, electrical, civil and petroleum industries [12, 13]. However, the

service temperature of TiNi SMA is limited to below 100 °C. Meanwhile, many applications such as smart rocket components, engine controls and high force actuators demand SMMs with both high temperature resistance and high recovery stress [14, 15].

Consequently, high temperature SMA (HTSMA) has attracted more and more interests in recent years [16, 17]. Among the HTSMAs, TiNiHf is very promising and it has been used in applications [16]. However, HTSMAs are very difficult to be obtained, because they are prepared through high-demanding furnaces at about 1000 °C with complicated procedures in most cases, while the yield is usually low [16–18]. Moreover, poor workability due to the ordered intermetallic structure of many HTSMA systems and high material costs pose additional problems for the commercialization of HTSMAs [19]. Compared with the numerous commercially available TiNi products, the products of HTSMAs are scarce, which hinders the development and application of high temperature SMMs greatly [19–21].

Shape memory polymers (SMPs) have become a noteworthy topic in recent years and most of them are samples with low to medium shape transition temperatures [22–24], while shape memory polyimide (SMPI) is a typical kind of high temperature SMP [25]. When the SMP was heated and deformed above its glass transition temperature (T_g), the elastic stress was generated and stored in the polymer chains at the temperature below T_g. When it was reheated above T_g under fixed constant strain, the polymer chains could move and the stored energy was released in the form of recovery stress [26, 27]. Although SMP possesses advantages such as easy processing and light weight over SMA, there is a large gap between recovery stresses of SMP and SMA [28–30]. According to the literature, the recovery stresses of SMPs and their composites are mainly 4–10 MPa, while the recovery stresses of HTSMAs mainly range from 100 to 500 MPa [12, 31, 32]. In fact, low recovery stress of SMPs is the main barrier that hinders their wide-spread applications. In order to enhance the mechanical properties and recovery stress of SMPs, various stiff fillers such as short carbon fibers, silicon carbide whiskers, and SiO_2 nanoparticles have been incorporated in SMP matrix to form SMP composites [31, 33, 34]. Moreover, there have been some attempts to combine NiTi SMA and SMP to form multifunctional smart material systems, and most of these composite structures include either SMA embedded in SMP, SMA wrapped around SMP, or SMA patterned on the surface of SMP [35]. The recovery force has increased from 7 N for pure polyurethane SMP belt to 12.8 N for the composite with NiTi SMA wire embedded in the SMP belt [36]. Although these composites exhibit mechanical properties and recovery stress higher than those of the pure SMPs, their recovery stresses are still much lower than those of SMAs [37].

Therefore, the main objective of the research is to offer a high temperature SMM with high recovery stress, convenient preparation methods, low cost and good workability. We have tried many fillers to increase the recovery stress of SMPI, and it is observed that silver fibers were unable to generate uniform SMPI composite since they precipitated in the curing process due to high density. The recovery stress of SMPI can be increased to 40.1 MPa through the reinforcement of short carbon fibers, but it is still much lower than those of HTSMAs [26]. Carbon fiber cloth (CFC) has been widely used as reinforcement of concrete in architectures such as floorslab, bridge and tunnels due to its good corrosion resistance, high strength, large elastic modulus and light weight [38]. By employing CFC as reinforcement, SMPI with high recovery stress (HRSMPI) at the level of HTSMAs is obtained. On considering the launching cost of about \$10 000 kg^{-1} in aerospace, HRSMPI is of special importance for aerospace since the low density can reduce the weight, thus saving the launching expense greatly when used in spacecrafts [39, 40]. Moreover, the workability of HRSMPI is demonstrated through a primitive actuator. The combination of high temperature shape memory effect, high recovery stress and low density guarantees HRSMPI great potential in many smart applications.

2. Experimental section

2.1. Materials

2-(4-Aminophenyl)-5-aminobenzoxazole (AAB) and bis phenol A dianhydride (BPADA) were purchased from Changzhou Sunlight Pharmaceutical Co., Ltd, and they were used directly. N,N-Dimethylacetamide (DMAc) was purchased from Sigma-Aldrich Co., Ltd, and it was distilled with activated molecular sieves to remove the residual water. CFC was purchased from Yancheng Xiang Sheng Carbon Fiber Technology Co. and it was dipped in the mixture of 1:1 alcohol/acetone for 2 h to remove the impurities, and then it was kept at 400 °C in air oven for 30 s to execute oxidation of the carbon fibers [41]. TiNiHf HTSMA ribbon was purchased from Hefei Kejing Material Technology Co. Ltd

2.2. Synthesis of pure SMPI and HRSMPI

15.8575 g AAB was added into a 1000 ml three-necked flask and dissolved in 300 ml DMAc under dry N_2 by mechanical stirring. 36.6547 g BPADA was added slowly into AAB solution under stirring, and the mixture was stirred for 10 h to form viscous poly(amic acid) (PAA). Such concentration is appropriate for the synthesis of HRSMPI, as higher concentration is too viscous to be handled while lower concentration is unable to infiltrate the CFC. After removing bubbles in vacuum at 60 °C for 10 h, PAA was cast onto glass substrate and then experienced step-wise curing at 90, 120, 150, 180, 210, 230, 260 and 300 °C for 1.5 h, respectively. The shorter dwelling time in vacuum furnace is unable to remove the bubbles completely, while longer dwelling time is unnecessary. The heating at 90, 120, 150 and 180 °C can remove the solvent, and PAA solution was solidified. The film imidized very little below 200 °C, and PAA was completely imidized into PI after further treatment at 210, 230, 260, and 300 °C [42, 43]. The single step curing will lead to residual solvent or microporosity or incomplete imidization, which will make the PI unsuitable for applications. The pure SMPI was removed from substrate in water and dried in air oven at 120 °C.

The PAA was poured into a glass square plate and CFC was dipped into the PAA solution in the plate for 40 h, then the CFC soaked with PAA was taken out from the plate and placed on a clear glass substrate. A KTQ film casting knife was employed to make uniform thickness, then the bubbles were eliminated in vacuum at 60 °C for 12 h. After undergoing the same curing steps of pure SMPI, HRSMPI was obtained and the weight content of SMPI was about 43%.

2.3. Characterizations

Fourier transform infrared spectra were obtained from 400 to 4000 cm^{-1} with Nicolet IS50 spectrometer, Thermo Scientific, USA. Raman spectroscopy was performed through Renishaw inVia Raman Microscope from 800 to 2500 cm^{-1}. The optical microscopy (OM) images were obtained with Zeiss Axio Imager A2m (Carl Zeiss AG, Germany). Scanning electron microscopy (SEM) images were characterized with ZEISS SUPRA55 (Carl Zeiss AG, Germany) at accelerating voltage of 10 kV, and the samples were coated with Au layer before observation. Mechanical properties were examined through tensile stress–strain behavior with Shimadzu Precision Universal Tester AG-X plus (Shimadzu Corporation, Japan) following the ASTM D882-02 standard technique, the sample was cut into 10 mm wide and 70 mm long strip with the gauge length of about 50 mm. The sample was fastened tightly and then stretched at the speed of 5 mm min^{-1} until it was broken, and the average of five duplicates was taken as the value of mechanical property. The analysis of variance on the mechanical properties was performed, and Tukey's test was used to obtain means comparisons. The three-point flexural test was performed according to ASTM D790M with Shimadzu Precision Universal Tester AG-X plus, the supporting span was 32 mm and the crosshead speed was 5 mm min^{-1}. The home-made instrument was employed to fix HRSMPI tightly with four screws, and the force normal to its surface was exerted until it was broken with Shimadzu Precision Universal Tester AG-X plus. Thermomechanical properties were characterized through dynamic mechanical analysis (DMA) with TA-Q800 (TA Instruments, New Castle, DE, USA) in tensile mode at the frequency of 1 Hz with heating rate of 3 °C min^{-1}, and the DMA measurement was performed in accordance with ASTM D5026. Thermal stability was examined through thermogravity analysis (TGA) under N_2 atmosphere with Mettler-Toledo TGA/SDTA851 (Mettler-Toledo International Inc., Switzerland) at the healing rate of 10 °C min^{-1} from room temperature to 800 °C. Thermal conductivity was measured through NETZSCH LFA 447 flash thermal conductivity meter, all specimens were round with diameter of 12.7 mm and the thin layer of graphite was applied to the surface of the specimen before testing.

Shape memory effect was determined with bending test, and the process was recorded with Canon VIXIA HF R500. The specimen was bent to bending angle (θ_b) at T_g + 20 °C, then it was cooled at room temperature to fix the temporary shape. The fixity angle (θ_f) was obtained after releasing the bending force, and shape fixity (R_f) was calculated with equation (1).

$$R_f = \frac{\theta_f}{\theta_b} \times 100\%. \quad (1)$$

When the bent sample was reheated to the shape memory temperature, it would return to its initial shape at recovery angle (θ_r), and shape recovery (R_r) was calculated with equation (2).

$$R_r = \frac{\theta_f - \theta_r}{\theta_f} \times 100\%. \quad (2)$$

Recovery stress was measured through INSTRON 5965 universal testing instrument equipped with Environmental Chamber 3119–506, the specimen was cut into 10 mm wide and 40 mm long strips with the gauge length of 20 mm. The recovery stress was obtained in the environmental chamber with the following procedures: (a) fasten the strip tightly at room temperature and heat it to T_g + 20 °C at 10 °C min^{-1}, then increase the stress to stretch HRSMPI and pure SMPI; (b) decrease the stress to fix the desired strain of 3.2% and 100% for HRSMPI and SMPI, respectively; (c) decrease the temperature to T_g − 120 °C at 10 °C min^{-1} under constant strain; (d) release the load and clamp the strip at T_g − 120 °C and (e) reheat the strip to T_g + 20 °C at 10 °C min^{-1} under constraint, and the stress obtained in this step is the recovery stress. The schematic diagram of the methodology of measuring recovery stress is expressed in figure 1.

2.4. Primitive actuator

The Schematic illustration of the primitive actuator made of HRSMPI and TiNiHf ribbon is shown in the supporting information as figure S1 (available online at stacks.iop.org/SMS/30/035027/mmedia), and the HRSMPI actuator was prepared with the following procedures: (a) the strip was bent into U shape in the position of its 1/3 length on the hot-stage set at T_g + 20 °C, and the shape was maintained at room temperature due to shape fixity; (b) a steel plate was placed on the lower section to fix the temporary shape and act as base of the primitive actuator, another metal sheet was placed on the upper section; (c) the temperature was increased to T_g + 20 °C and HRSMPI could overturn the metal sheet on its upper section; (d) HRSMPI completely overturned the metal sheet due to shape recovery like a primitive actuator.

The similar procedures were employed to prepare primitive actuator made of TiNiHf ribbon, and TiNiHf actuator could also overturn metal sheet with shape recovery temperature of 130 °C.

3. Results and discussions

3.1. Synthesis, morphology and structure

The pure SMPI is synthesized by two-step condensation polymerization of BPADA and AAB, and the as-prepared HRSMPI is a rigid thin sheet composed of SMPI and CFC, as shown in figure 2. Compared with the high-demanding devices and complex metal smelting procedures of HTSMA, HRSMPI can be prepared with common devices and simple procedures.

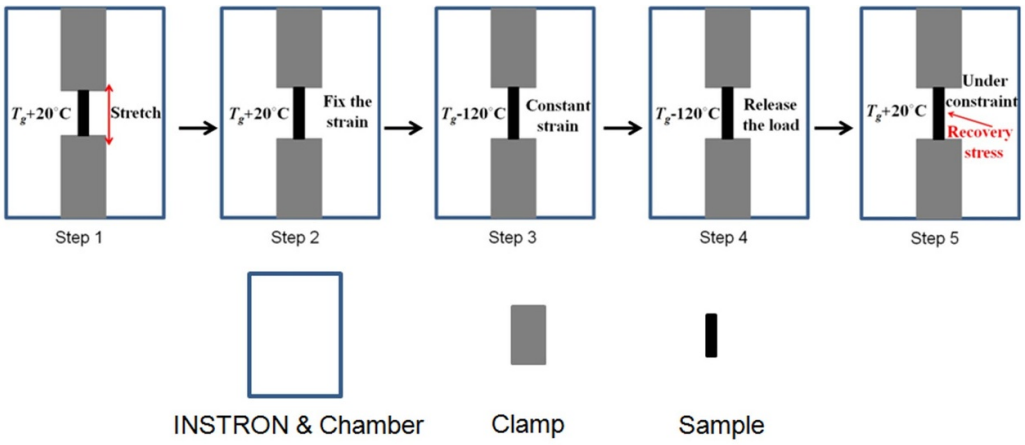

Figure 1. Schematic diagram of the methodology of measuring recovery stress.

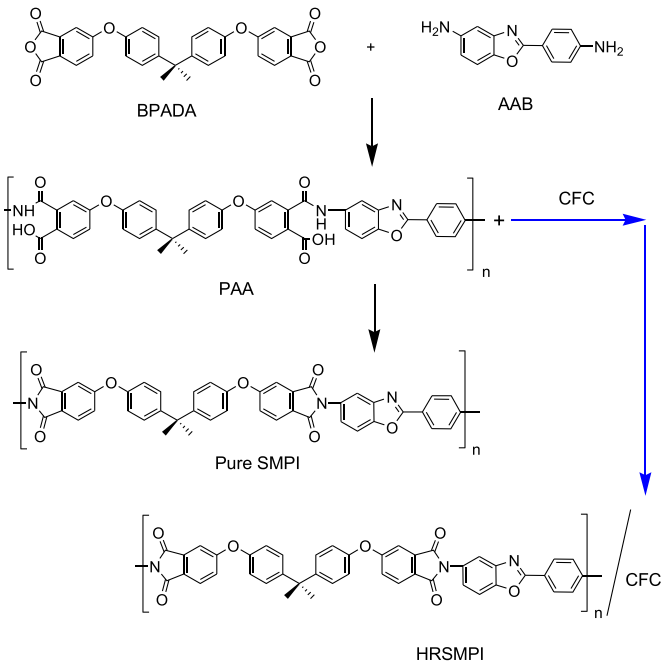

Figure 2. Synthesis of pure SMPI and HRSMPI.

The morphology of HRSMPI is studied and it possesses a unique sandwich structure, as shown in figure 3. The macroscale morphology indicates that the two-dimensional interwoven longitudinal and horizontal carbon fiber bundles act as the skeleton of HRSMPI, and the space outside the fiber bundles was filled with SMPI resin (figure 3(a)). The OM image demonstrates that carbon fibers are tightly packed inside the fiber bundle (figure 3(b)), and the SEM image indicates that the carbon fibers are embedded in SMPI resin on the surface (figure 3(c)). The cross-section image demonstrates that HRSMPI possesses a unique sandwich structure (figure 3(d)). Its bottom layer is pure SMPI, the intermediate layer is the resin filled with carbon fibers, and the top layer is thin SMPI film. Further study demonstrates that carbon fibers are not pulled out from SMPI resin (figures 3(e) and (f)), indicating that there is nice compatibility between SMPI resin and carbon fibers due to the oxidation of CFC [41].

The sandwich structure of HRSMPI is caused by its preparation method, as it is obtained through the imidization of PAA into SMPI with the existence of CFC. The densities of PAA and SMPI are higher than that of carbon fibers, which leads to the formation of SMPI bottom layer. The strong affinity between carbon fibers and the highly viscous resin has hindered fast upward floating of CFC, and thus the intermediate layer filled with carbon fibers was formed. The CFC has been dipped in PAA solution before thermal curing, and the soaked PAA can form thin SMPI layer on the surface. As a result, the sandwich structure is obtained in HRSMPI.

The structures of pure SMPI and HRSMPI are further characterized with IR and Raman, as shown in figure 4. The characteristic peaks of polyimide such as asymmetric stretching of Ar–C–O (1253 cm^{-1}), stretching of –C–N (1370 cm^{-1}), symmetric and asymmetric stretching of imide carbonyl (1719 cm^{-1} and 1777 cm^{-1}) are observed in both pure SMPI and HRSMPI (figure 4(a)), indicating that both pure SMPI and HRSMPI are completely imidized [44, 45]. Compared with pure SMPI, HRSMPI exhibits an enhanced IR peak at about 1620 cm^{-1} due to the stretching vibration of C=C in carbon fibers [26]. The pure SMPI exhibits the characteristic Raman peaks of polyimide, and the corresponding vibrations of C=O, C=C and C–N–C are located at 1786 cm^{-1}, 1627 cm^{-1} and 1387 cm^{-1}, respectively [46]. These peaks are also observed in HRSMPI, indicating that both pure SMPI and HRSMPI are completely imidized (figure 4(b)). The Raman spectra of CFC are shown in the supporting information as figure S2, and the overlapping of Raman peaks of polyimide and CFC is quite obvious in HRSMPI. The IR and Raman spectra indicate that the imidization of HRSMPI is completed in the existence of CFC.

3.2. *Mechanical and thermal properties*

Tensile test is commonly used to study mechanical properties of polymers, and the mechanical properties of pure SMPI and HRSMPI are characterized through tensile stress–strain

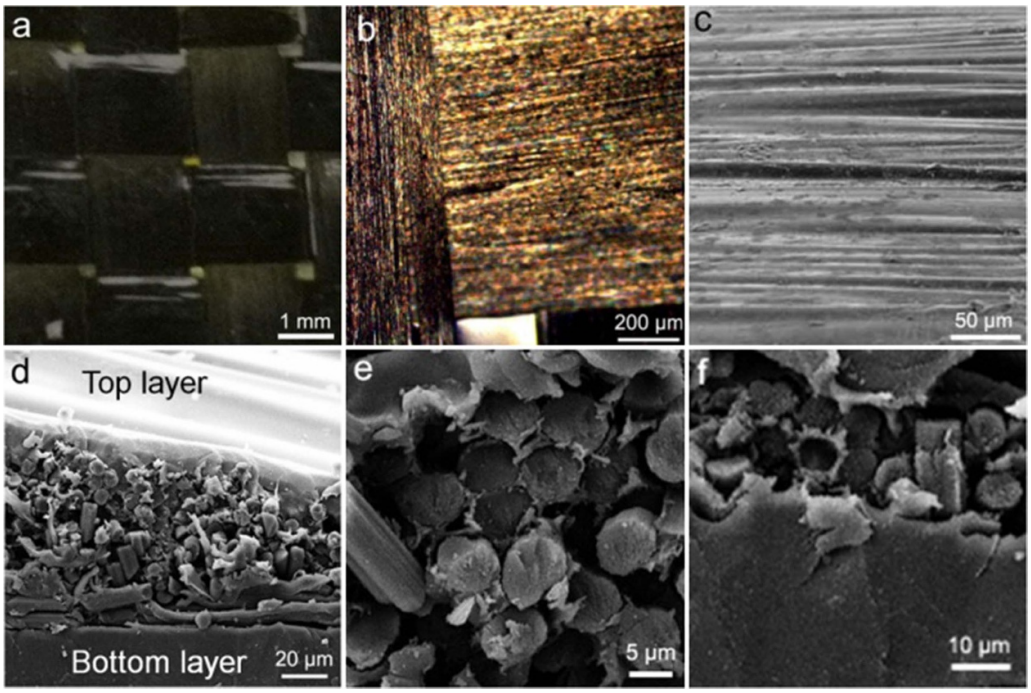

Figure 3. Morphology of HRSMPI. Macroscale image (a), OM image (b), SEM image of surface (c), its cross-section image (d), magnified image of the intermediate layer (e) and bottom layer (f).

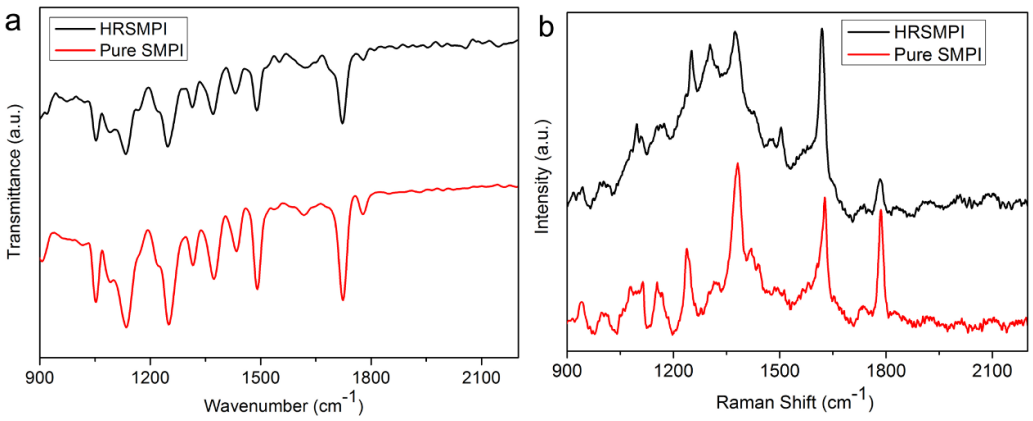

Figure 4. FT-IR (a) and Raman spectroscopy (b) of pure SMPI and HRSMPI.

behaviors, as shown in figure 5(a). The pure SMPI manifests gradual failure in ductile manner and its stress exhibits non-linear behavior as the strain increases similar to some other polyimides, and this behavior is also ascribed to ductility of this polyimide [45]. Meanwhile, HRSMPI exhibits sudden failure in brittle manner and its stress manifests linear behavior with the increase of strain. The macroscale image of HRSMPI after stress–strain test indicates that it underwent a sudden failure (figure 5(b)), and the microstructure of the fracture demonstrates that the carbon fibers are broken rather than stretched out from the matrix (figure 5(c)). Therefore, the sudden brittle behavior in stress–strain curve of HRSMPI is determined by the microstructure of the fracture. It has been observed that the fracture features of carbon fiber reinforced polymer composites mostly depend on the interfacial bonding, and the composites with good interfacial bonding between polymer matrix and carbon fiber fillers such as the aerospace grade epoxy composite exhibit brittle fracture under tension [47, 48]. The brittle fracture also indicates good interfacial bonding between SMPI matrix and CFC filler in HRSMPI.

The pure SMPI shows Young's modulus of 2.28 ± 0.32 GPa, maximum tensile stress of 122 ± 9 MPa and elongation at break of $15.1 \pm 1.7\%$, respectively. In comparison, HRSMPI possesses Young's modulus of 11.5 ± 1.2 GPa, maximum tensile stress of 413 ± 22 MPa and elongation at break of $3.6 \pm 0.3\%$, respectively. Young's modulus of HRSMPI is four times higher than that of pure SMPI, indicating that CFC can increase the stiffness of polyimide resin greatly like other polymer composites [31, 38]. The tensile stress of HRSMPI is 2.4 times higher than that of pure SMPI, since the good interfacial affinity can lead to effective stress transfer from SMPI resin to CFC, while CFC plays the role

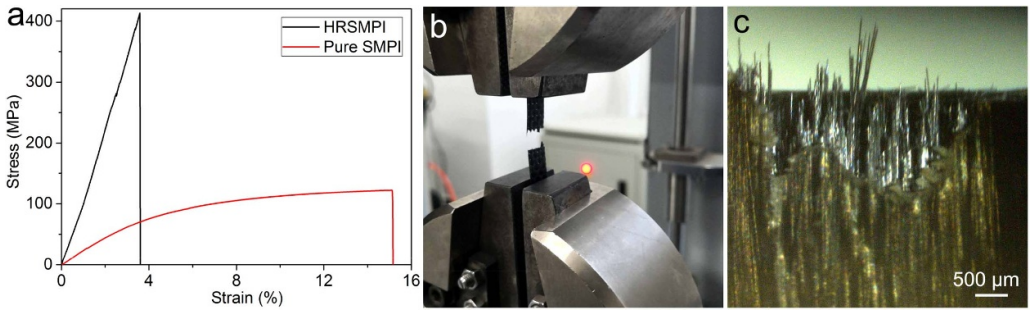

Figure 5. Tensile stress–strain behaviors of HRSMPI and pure SMPI (a), macroscale image of HRSMPI after stress–strain test (b), and microstructure of the fracture (c).

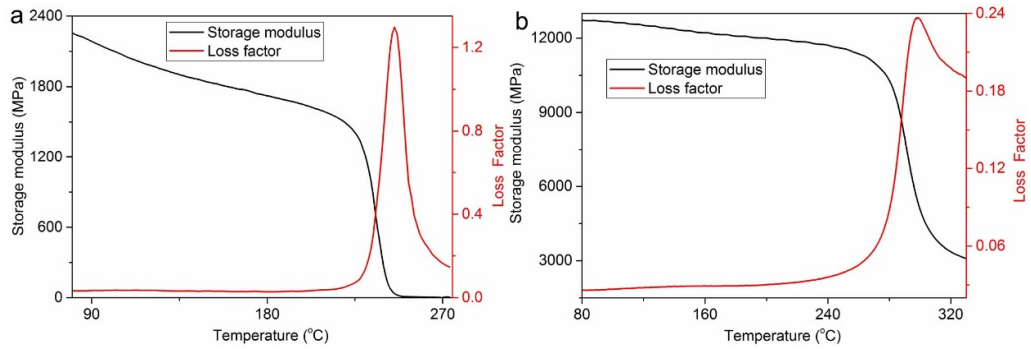

Figure 6. Thermomechanical properties of pure SMPI (a) and HRSMPI (b).

of skeleton in HRSMPI and mainly carries the applied stress [11, 49, 50]. The elongation at break of HRSMPI is lower than that of pure SMPI, as CFC has much lower elongation than polymer resins [51, 52]. For HRSMPI, the recommended safe working range is about 3% strain level to avoid fracture and keep its integrity.

Three-point flexural test has been employed to study mechanical properties of thick polymer samples with thickness of several micrometers (mm), and they were damaged to obtain the flexural strength in the test [49]. The thickness of HRSMPI is much lower than 1 mm, and it remained intact after the test, as shown in the supporting information (figure S3). Since the three-point flexural test was unable to damage HRSMPI, the home-made instrument was employed to fix HRSMPI tightly and damage it (figure S4(a)). The fracture of HRSMPI is rather uniform (figure S4(b)), further indicating that there is strong bonding between CFC and the matrix. The carbon fiber bundle underwent catastrophic failure in the bending side (figure S4(c)), suggesting that the external force is mainly carried by the carbon fiber bundles.

HRSMPI is more thermally stable than pure SMPI, as shown by their TGA spectra in the supporting information (figure S5). The temperature at which 5% weight loss occurs is taken as decomposition temperature (T_d), and T_d of pure SMPI and HRSMPI are 548 °C and 602 °C, respectively. The increase of T_d is caused by CFC, as carbon fibers are highly thermally stable. The solid residue of pure SMPI and HRSMPI at 800 °C are 58.2% and 75.8%, respectively. The higher residue of HRSMPI is caused by the barrier effect of CFC, which can act as thermal cover layer to reduce the escaping rate of pyrolysis products [53].

3.3. Thermomechanical properties

The thermomechanical properties of pure SMPI and HRSMPI are analyzed with DMA, as shown in figure 6. The peak of loss factor (tan δ) is usually taken as T_g of polyimide, and the T_g of pure SMPI is 245 °C (figure 6(a)). The storage modulus (E') of pure SMPI decreases slowly with the increase of temperature in glassy state, but it undergoes a huge drop during glass transition process and E' at 225 °C (T_g − 20 °C, glassy state) and 265 °C (T_g + 20 °C, rubbery state) are 1.41 GPa and 3.98 MPa, respectively. T_g of HRSMPI is 300 °C, while its E' at 280 °C and 320 °C are 10.28 GPa and 3.36 GPa (figure 6(b)), respectively.

T_g is closely correlated with chain segments motion and the highly increased T_g of HRSMPI is mainly caused by the carbon fibers in CFC, which could obstruct the chain movements of SMPI molecules [51]. The peak height of tan δ is associated with damping capability, and the decreased peak height of HRSMPI is due to the incorporation of CFC. The width of tan δ is correlated with network homogeneity, and the carbon fibers would inevitably make the distribution of molecular weight become wider [51–53]. As a result, the width at half height of tan δ of HRSMPI is larger than that of pure SMPI. The CFC can increase the E' of HRSMPI in glassy state greatly, while mainly determine its E' in rubbery state.

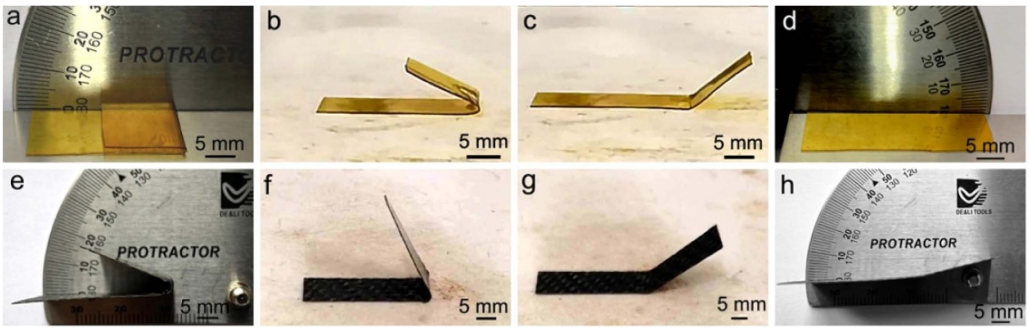

Figure 7. Shape memory effects of pure SMPI and HRSMPI. Shape fixity (a), images on 265 °C hot-stage at 9 s (b) and 18 s (c), and shape recovery of pure SMPI (d); shape fixity (e), images on 320 °C hot-stage at 5 s (f) and 13 s (g), and shape recovery of HRSMPI (h).

3.4. Shape memory performance

The shape memory performances of pure SMPI and HRSMPI have been studied, as manifested in figure 7. The pure SMPI can be bent into temporary shape easily at 265 °C and then fix the temporary shape completely at room temperature with R_f of 100% (figure 7(a)). It will return to its initial shape when reheated, and the images on 265 °C hot-stage at 9 s and 18 s are manifested in figures 7(b) and (c), respectively. It will return to its initial shape completely with R_r of 100% after 23 s (figure 7(d)), and the video recording this process is supplied in the supporting information as video S1.

The E' in glassy state of pure SMPI (1.41 GPa) is 353 times higher than that in rubbery state (3.98 MPa), and the large increase in E' can effectively freeze chain mobility and fix the temporary shape with high R_f when cooled [44]. The complete shape recovery indicates that its permanent phase composed of chain entanglements and strong π–π intermolecular interactions is strong enough to maintain the original shape [9, 45]. Unlike the pure SMPI, E' in glassy state of HRSMPI (10.28 GPa) is just 2.06 times higher than that in rubbery state (3.36 GPa), and the comparatively small difference in E' leads to its R_f of 90.6% (figure 7(e)) [44]. The images of its shape recovery on 320 °C hot-stage at 9 s and 15 s are illustrated in figures 7(f) and (g), respectively. The carbon fibers in CFC can obstruct chain mobility of polyimides in HRSMPI, which would hinder its complete shape recovery and lead to R_r of 92.2% after 21 s (figure 7(h)) [26]. The video showing shape recovery of HRSMPI is supplied in the supporting information as video S2.

SMP has historically lagged behind SMA due to its low stiffness, low recovery stress, poor fatigue characteristics, etc [32, 54]. Recovery rate is the rate at which SMP can return to its maximum recovery shape, and it is closely related with the width of thermal transition at phase transition temperature (T_{trans}) and thermal conductivity of SMP. The wider thermal transition and lower thermal conductivity can lead to slower recovery rate [27]. The incorporation of CFC has led to wider thermal transition of HRSMPI at T_g, as demonstrated in the DMA spectra (figure 6). Meanwhile, CFC has enhanced the thermal conductivity from 0.135 W m^{-1} K^{-1} of pure SMPI to 0.217 W m^{-1} K^{-1} of HRSMPI. The positive effect of increased thermal conductivity prevails the negative effect of wider thermal transition, and thus HRSMPI exhibits higher recovery rate (21 s) than that of pure SMPI (23 s).

3.5. Recovery stress behavior

The elastic strain energy of SMP generated during shape deformation is stored in the temporary shape when cooled, and the stored strain energy will be released in the form of recovery stress when the SMP is reheated under constraint [31]. The shape recovery of SMPI was usually performed at T_g + 20 °C [26, 45], and here the recovery stresses of pure SMPI and HRSMPI are also characterized at T_g + 20 °C, as shown in figure 8. The stress of pure SMPI is almost constant with strains higher than 100% at T_g + 20 °C, while HRSMPI with strains higher than 3.2% will produce bad shape recovery. Therefore, the strains of pure SMPI and HRSMPI are set as 100% and 3.2%, respectively. The HRSMPI was heated to 320 °C and stretched with tensile stress of 350 MPa (step 1), then the stress decreased to fix the strain (step 2). When it was cooled under constant strain, the stress increased to 387 MPa with the decrease of temperature (step 3). After releasing the load (step 4), HRSMPI was reheated to 320 °C under constraint and the stress gets higher with the increase of heating time before reaching the maximum value and then decreases with further heating (step 5). The recovery stress of HRSMPI is 116 MPa, as shown in figure 8(a). In comparison, the pure SMPI exhibits recovery stress of 6.8 MPa (figure 8(b)). Therefore, the high recovery stress of HRSMPI is mainly caused by CFC, which can store more elastic strain energy and then release it in the form of high recovery stress.

Although HRSMPI shows similar recover stress variation trend like those reported such as the SMP reinforced with SiC whiskers (SMP/SiC_w), the recovery stress of 116 MPa for HRSMPI is much higher than the 11.2 MPa for SMP/SiC_w [31]. The recovery stress of HRSMPI is at the level of HTSMA, as the recovery stresses of FeMnSiCrNi and annealed FeMnSi alloys are 120 MPa and 110 MPa, respectively [19, 20].

3.6. Primitive actuator performance

In order to demonstrate the high recovery stress of HRSMPI in a more practical way, 0.2946 g HRSMPI strip was processed

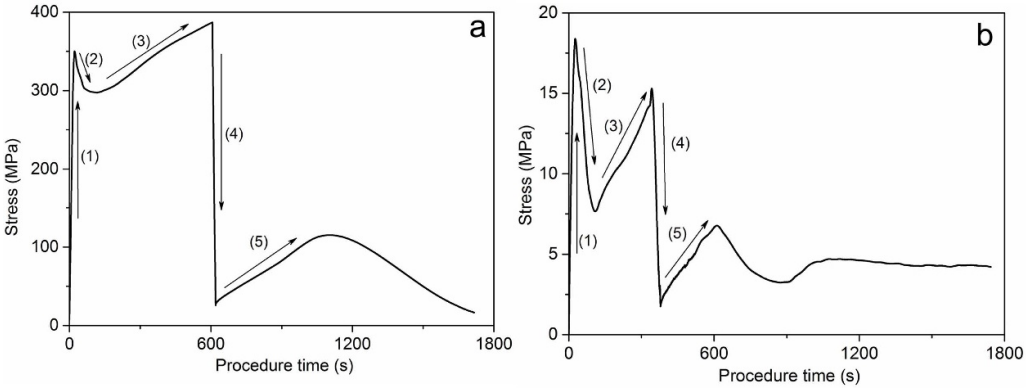

Figure 8. Recovery stresses of HRSMPI (a) and pure SMPI (b). (1) Stretching at $T_g + 20$ °C, (2) fixing strain at 20 °C, (3) cooling under constant strain, (4) removing the stress and (5) reheating under constraint.

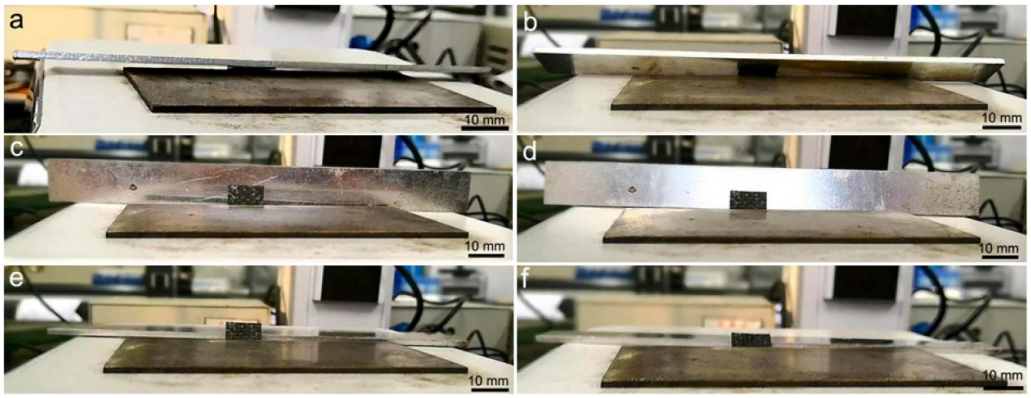

Figure 9. Primitive actuator made of 0.2946 g HRSMPI overturning 43.51 g Al sheet. The images on 320 °C hot-stage at 0 s (a), 48 s (b), 69 s (c), 71 s (d), 72 s (e), and 73 s (f).

into a primitive actuator following the procedures in the experimental section, and its performance was shown in figure 9. The 43.51 g Al sheet was placed on the actuator (figure 9(a)), and the actuator could overturn the Al sheet upon heating. The images on 320 °C hot-stage at 48 s, 69 s, 71 s, 72 s and 73 s are illustrated in figure 9(b) to figure 9(f), respectively. The video recording this process is supplied in the supporting information as video S3, while the actuator made of pure SMPI was unable to overturn the metal sheet due to its low recovery stress. The suitable weight content of SMPI in HRSMPI is about 43%, as higher content leads to lower recovery stress while lower content results in worse shape memory effects. For example, the composite with 51% SMPI was unable to overturn the same Al sheet as HRSMPI, and it could overturn another Al sheet 102 times heavier than its own weight, and this process is supplied in the supporting information as video S4. The CFC does not have shape memory effects, and the composite with 38% SMPI exhibited decreased shape fixity of 80% and shape recovery of 78%, as shown in the supporting information (figure S6).

Shape memory cycle time represents the overall time necessary for the programming of temporary shape and recovery of permanent shape of SMP materials [27]. In free shape recovery of HRSMPI, it takes 5 min to soften the specimen, 1.5 min to program the temporary shape, 20 s to recover the shape, and the shape memory cycle time is 410 s. In the primitive actuator, it takes 5 min to soften the specimen, 1.5 min to program the temporary shape, 75 s to recover the shape, and the shape memory cycle time is 475 s. Compared with free shape recovery, metal sheet on the actuator can hinder movements of polyimide chains greatly and thus leads to longer shape memory cycle time.

The commercial TiNiHf HTSMA was employed as reference, and the performance of primitive actuator made of TiNiHf ribbon was shown in figure 10. The 0.0126 g TiNiHf can overturn 2.0107 g steel sheet, and the images on hot-stage at 0 s, 12 s, 23 s, 29 s, 38 s and 39 s are illustrated in figures 10(a)–(f), respectively. The video recording this process is supplied in the supporting information as video S5, and the TiNiHf ribbon can overturn the object 159 times heavier than its own weight. HRSMPI exhibits similar performance, as HRSMPI strip can overturn the metal sheet 147 times heavier than itself. Meanwhile, the density of HRSMPI is 0.96 g cm^{-3}, less than 1/6 of the 6.5 g cm^{-3} density of TiNiHf HTSMA [18].

Due to its high recovery stress and low density, HRSMPI has great potentials in applications such as high force actuators, high temperature seals and smart jet propulsions. Besides, it is also a possible candidate for lightweight alternative to HTSMA in some cases. High reliability is very important for

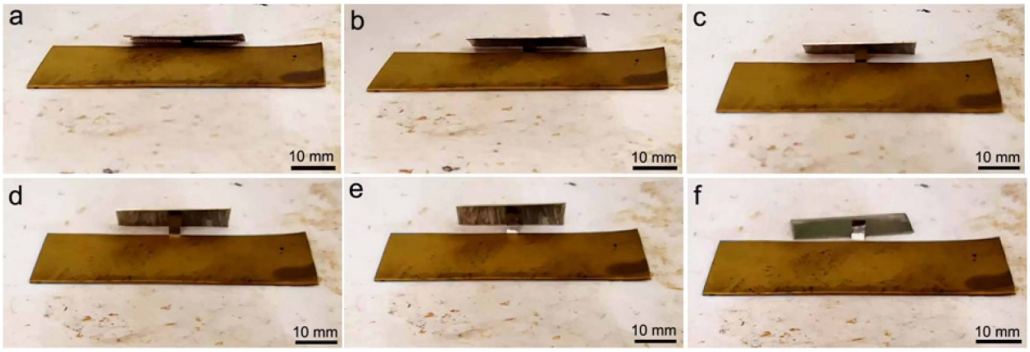

Figure 10. Primitive actuator made of 0.0126 g TiNiHf ribbon overturning 2.0107 g steel sheet. Their images on hot-stage at 0 s (a), 12 s (b), 23 s (c), 29 s (d), 38 s (e), and 39 s (f).

Table 1. Comparison of NiTi SMA, HTSMAs, epoxy SMP, SMPI and HRSMPI.

Material/property	SMA	HTSMAs	SMP	SMPI	HRSMPI
Density (g cm^{-3})	6.4–6.5	5.3–6.8	0.9–1.1	1.41–1.57	0.94–0.98
Typical transformation range (°C)	−50–100	100–400	−10–130	180–380	310–350
Observed phase transformation	A⇄M, R-phase	A⇄M, R-phase	Glass transition	Glass transition	Glass transition
Free recovery speed (s)	<1	∼1	30–150	5–30	5–20
Recovery stress (MPa)	200–760	100–500	1–3	2–6	100–116
Shaping	Difficult	Very difficult	Easy	Moderate	Moderate
Cost in $/1b	∼250	∼3200	<10	∼750	∼950

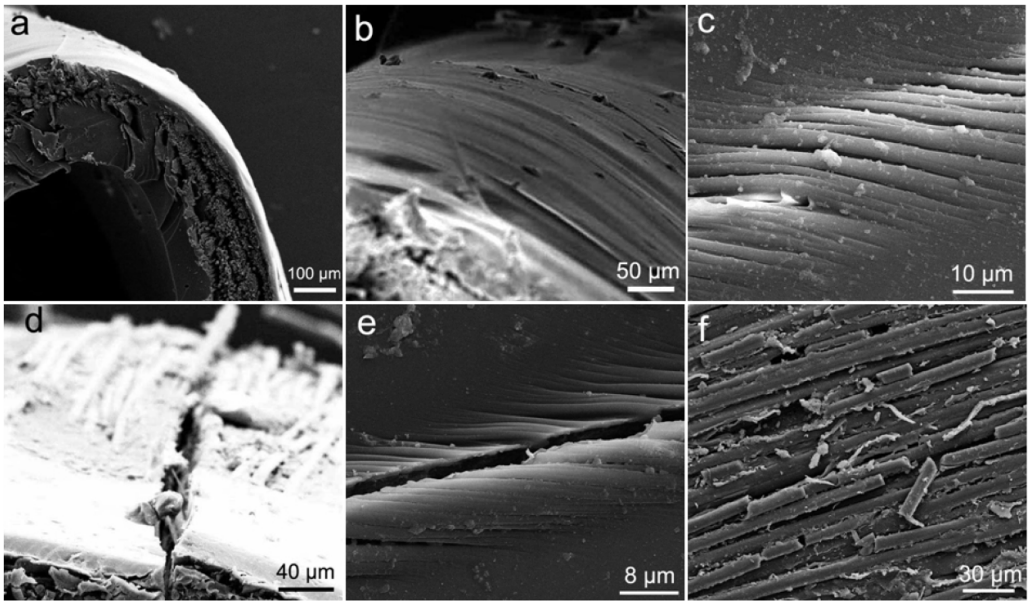

Figure 11. SEM images of HRSMPI before (a)–(c) and after (d)–(f) overturning the metal sheet through shape recovery from bending deformation.

practical applications, and the reliability of HRSMPI is verified by multiple samples tested. Another HRSMPI actuator can also overturn the same Al sheet, as shown in the supplemental information (video S6). Moreover, it will take less time for HRSMPI actuator to overturn the lighter metal sheet like many other actuators in practice, and the faster actuators are shown in the supplemental information (videos S7 and S8). The multiple actuators have confirmed the high reliability of HRSMPI. The basic properties of NiTi SAM, HTSMA, epoxy SMP, SMPI and HRSMPI are compared in table 1 [1, 12, 28, 37, 55–57].

3.7. Mechanism of high recovery stress

The above-mentioned results have demonstrated that the recovery stress of HRSMPI is predominated by CFC, and the possible mechanism is discussed on the basis of the SEM images in figure 11. The primitive actuator is based on bending

deformation, and HRSMPI was bent into an arch bridge shape (figure 11(a)). The image of curvature surface demonstrates that the carbon fiber bundle is well bended without breakage (figure 11(b)), and the magnified image indicates that the carbon fiber bundle is taut tightly in the bending area (figure 11(c)). After overturning the metal sheet through shape recovery, there is an obvious crack in the bending area of HRSMPI (figure 11(d)), and further analysis indicates that the carbon fiber bundle in the bending area is broken uniformly (figure 11(e)), while the carbon fibers in other areas are broken sporadically (figure 11(f)). The reused HRSMPI can no longer overturn metal sheet in the same bending area. In a device conceived for one-time activation (i.e. micro-actuator for satellite), repeated cycles are not needed [58], and HRSMPI have vast potential in such applications. In comparison, free shape recovery of HRSMPI will not lead to crack of carbon fibers.

These results indicate that elastic strain energy generated during shape deformation of HRSMPI is mainly stored in carbon fiber bundles, the stored energy is released as recovery stress under constrained shape recovery, and the release of recovery stress leads to fracture of the carbon fiber bundles.

4. Conclusion

In summary, SMPI composite with recovery stress at the level of HTSMA is obtained through common devices and simple procedures. The HRSMPI is composed of 43% SMPI resin and CFC, and it is prepared in the common furnace of chemistry lab with ultimate curing temperature of 300 °C. The HRSMPI possesses unique sandwich structure, Young's modulus of 11.5 ± 1.2 GPa, maximum tensile stress of 413 ± 22 MPa and elongation at break of 3.6 ± 0.3%, respectively. There is good interfacial bonding between SMPI matrix and CFC filler, and HRSMPI experienced brittle fracture under stretching. HRSMPI is suitable for high temperature shape memory applications as it exhibits high T_g of 300 °C, shape fixity of 90.6% and shape recovery of 92.2%. HRSMPI produces high recovery stress of 116 MPa, and the elastic strain energy generated during shape deformation is mainly stored in CFC, as the pure SMPI without CFC filler possesses low recovery stress of 6.8 MPa. Its good workability is demonstrated and the primitive actuator made of HRSMPI can overturn the metal sheet 147 times heavier than itself, similar to that made of commercial TiNiHf HTSMA. Meanwhile, the low density of 0.96 g cm^{-3} for HRSMPI is less than 1/6 of that for TiNiHf alloy. HRSMPI possesses great potential in high temperature smart applications due to its convenient preparation and outstanding properties, and it can also be a lightweight alternative to some HTSMA products conceived for one-time activation.

Acknowledgments

This work is financially supported by Natural Science Foundation of Heilongjiang Province (LC2018023), Science and Technology Innovation Program for Talents of Harbin (2017RALXJ004).

Supplemental information

The Schematic illustration of the preparation of primitive actuator, three-point flexural test of HRSMPI, the home-made instrument to characterize HRSMPI, TGA spectra of pure SMPI and HRSMPI, Raman spectroscopy of CFC, the videos recording shape recovery processes of pure SMPI and HRSMPI, as well as the videos recording primitive actuator performances of HRSMPI and TiNiHf HTSMA are shown in the supporting information.

ORCID iD

Xinli Xiao https://orcid.org/0000-0002-3383-2394

References

[1] Clark P W, Aiken I D, Kelly J M, Higashino M and Krumme R 1995 *Proc. SPIE* 2445
[2] Lendlein A and Langer R 2002 *Science* **296** 1673–6
[3] Patil D and Song G 2017 *Smart Mater. Struct.* **26** 093003
[4] Zhang J, Zheng X, Wu F, Yan B, Zhou S, Qu S and Weng J 2016 *ACS Macro Lett.* **5** 1317–21
[5] Wu F, Jin L, Zheng X, Yan B, Tang P, Yang H, Deng W and Yang W 2017 *ACS Appl. Mater. Interfaces* **9** 38323–35
[6] Tang P, Zheng X, Yang H, He J, Zheng Z, Yang W and Zhou S 2019 *ACS Appl. Mater. Interfaces* **11** 48202–11
[7] Ze Q, Kuang X, Wu S, Wong J, Montgomery S, Zhang R, Kovitz J, Yang F, Qi H and Zhao R 2020 *Adv. Mater.* **32** 1906657
[8] Zhao Q, Qi H J and Xie T 2015 *Prog. Polym. Sci.* **49-50** 79–120
[9] Yang X T, Guo Y Q, Luo X, Zheng N, Ma T B, Tan J J, Li C M, Zhang Q Y and Gu J W 2018 *Compos. Sci. Technol.* **164** 59–64
[10] Kuang X, Chen K, Dunn C K, Wu J, Li V C F and Qi H J 2018 *ACS Appl. Mater. Interfaces* **10** 7381–8
[11] Liu Y P, Gall K, Dunn M L and McCluskey P 2004 *Mech. Mater.* **36** 929–40
[12] Li D S, Zhang X P, Xiong Z P and Mai Y W 2010 *J. Alloys Compd.* **490** L15–9
[13] Hartl D J and Lagoudas D C 2007 *Proc. Inst. Mech. Eng.* **221** 535–52
[14] Wen Y H, Li N and Xiong L R 2005 *Mater. Sci. Eng.* A **407** 31–5
[15] Sutou Y, Omori T, Wang J, Kainuma R and Ishida K 2004 *Mater. Sci. Eng.* A **378** 278–82
[16] König D, Zarnetta R, Savan A, Brunken H and Ludwig A 2011 *Acta Mater.* **59** 3267–75
[17] Khan M I, Kim H Y and Miyazaki S 2015 *Shape Mem. Superelasticity* **1** 85–106
[18] Kovarik L, Yang F, Garg A, Diercks D, Kaufman M, Noebe R D and Mills M J 2010 *Acta Mater.* **58** 4660–73
[19] Wang G, Peng H, Sun P, Wang S and Wen Y 2016 *Mater. Sci. Eng.* A **657** 339–46
[20] Kima Y, Han S, Choi E and Kima W 2017 *Mater. Sci. Eng.* A **701** 285–8
[21] Meng X, Cai W, Fu Y, Zhang J and Zhao L 2010 *Acta Mater.* **58** 3751–63

[22] Jin X D, Ni Q Q and Natsuki T 2011 *J. Compos. Mater.* **45** 2547–54
[23] Shi Y, Yoonessi M and Weiss R A 2013 *Macromolecules* **46** 4160–7
[24] Quitmann D, Reinders F M, Heuwers B, Katzenberg F and Tiller J C 2015 *ACS Appl. Mater. Interfaces* **7** 1486–90
[25] Koerner H, Strong R J, Smith M L, Wang D H, Tan L S, Lee K M, White T J and Vaia R A 2013 *Polymer* **54** 391–402
[26] Li X, Wang L, Zhang Z, Kong D, Ao X and Xiao X 2019 *Macromol. Chem. Phys.* **220** 1900164
[27] Rousseau I A 2008 *Polym. Eng. Sci.* **48** 2075–89
[28] Zheng N, Fang Z, Zou W, Zhao Q and Xie T 2016 *Angew. Chem.* **55** 11421–5
[29] Yan B Y, Zheng X T, Tang P D, Yang H K, He J and Zhou S B 2018 *ACS Appl. Mater. Interfaces* **10** 36249–58
[30] Narayana H, Hu J L, Kumar B, Shang S, Han J, Liu P, Lin T, Ji F and Zhu Y 2017 *J. Mater. Chem.* B **5** 1905–16
[31] Likitaporn C, Mora P, Tiptipakorn S and Rimdusit S 2018 *J. Intell. Mater. Syst. Struct.* **29** 388–96
[32] Liu C, Qin H and Mather P T 2007 *J. Mater. Chem.* A **17** 1543–58
[33] Madbouly S A and Lendlein A 2009 *Advances in Polymer Science* vol 226 (Berlin: Springer)
[34] Lu H, Yu K, Liu Y and Leng J 2010 *Smart Mater. Struct.* **19** 065014
[35] Tobushi H, Hayashi S, Hoshio K, Makino Y and Miwa N 2006 *Int. J. Adv. Manuf. Technol.* **17** 1075–81
[36] Ghosh P, Rao A and Srinivasa A R 2013 *Mater. Des.* **44** 164–71
[37] Ni Q Q, Zhang C, Fu Y, Dai G and Kimura T 2007 *Compos. Struct.* **82** 176–84
[38] Nakaso K, Teshima H, Yoshimura A, Nogami S, Hamada Y and Fukai J 2008 *Chem. Eng. Process.* **47** 879–85
[39] Bouwmeester J and Guo J 2010 *Acta Astronaut.* **67** 854–62
[40] Gagne K R, McDevitt M R and Hitt D L 2018 *Aerospace* **5** 52
[41] Wang Y and Wu G 2007 *New Carbon Mater.* 88–91
[42] Yan L, Park C, Ounaies Z and Irene E A 2006 *Polymer* **47** 2822–9
[43] Jo B W, Ahn K H and Lee S J 2014 *Polymer* **55** 5829–36
[44] Qiu X Y, Xiao X L, Kong D Y, Zhang W B and Ma Z J 2017 *J. Appl. Polym. Sci.* **134** 44902
[45] Wang Q H, Bai Y K, Chen Y, Ju J P, Zheng F and Wang T M 2015 *J. Mater. Chem.* A **3** 352–9
[46] Kadiyala A K, Sharma M and Bijwe J 2016 *Mater. Des.* **109** 622–33
[47] Yuan S, Zhang C, Amin M, Fan H and Liu M 2015 *Int. J. Adv. Manuf. Technol.* **81** 1223–31
[48] Kumar M S, Raghavendra K, Venkataswamy M A and Ramachandra H V 2012 *Mater. Res.* **15** 990–7
[49] Hine P J, Bonner M, Ward I M, Swolfs Y, Verpoest I and Mierzwa A 2014 *Composites* A **65** 19–26
[50] Liu D, Fleck N A and Sutcliffe M P F 2004 *J. Mech. Phys. Solids* **52** 1481–505
[51] Czél G, Jalalvand M and Wisnom M R 2016 *Compos. Struct.* **143** 362–70
[52] Diao H, Robinson P, Wisnom M R and Bismarck A 2016 *Composites* A **87** 186–93
[53] Shi P L, Schach R, Munch E, Montes H and Lequeux F 2013 *Macromolecules* **46** 3611–20
[54] Ma J, Karaman I and Noebe R D 2010 *Int. Mater. Rev.* **55** 257–315
[55] Leng J, Lan X, Liu Y and Du S 2011 *Prog. Mater. Sci.* **56** 1077–135
[56] Kong D and Xiao X 2016 *Sci. Rep.* **6** 33610
[57] Ao X, Kong D, Zhang Z and Xiao X 2020 *J. Mater. Sci.* **55** 4292–302
[58] Costanza G and Tata M E 2020 *Materials* **13** 1856